Loss of GET pathway orthologs in *Arabidopsis thaliana* causes root hair growth defects and affects SNARE abundance

Shuping Xing[a], Dietmar Gerald Mehlhorn[a], Niklas Wallmeroth[a], Lisa Yasmin Asseck[a], Ritwika Kar[a], Alessa Voss[a], Philipp Denninger[b], Vanessa Aphaia Fiona Schmidt[b], Markus Schwarzländer[c], York-Dieter Stierhof[d], Guido Grossmann[b], and Christopher Grefen[a,1]

[a]Centre for Plant Molecular Biology, Developmental Genetics, University of Tübingen, 72076 Tuebingen, Germany; [b]Centre for Organismal Studies, CellNetworks Excellence Cluster, University of Heidelberg, 69120 Heidelberg, Germany; [c]Institute of Crop Science and Resource Conservation, University of Bonn, 53113 Bonn, Germany; and [d]Centre for Plant Molecular Biology, Microscopy, University of Tübingen, 72076 Tuebingen, Germany

Edited by Natasha V. Raikhel, Center for Plant Cell Biology, Riverside, CA, and approved December 19, 2016 (received for review November 28, 2016)

Soluble *N*-ethylmaleimide–sensitive factor attachment protein receptor (SNARE) proteins are key players in cellular trafficking and coordinate vital cellular processes, such as cytokinesis, pathogen defense, and ion transport regulation. With few exceptions, SNAREs are tail-anchored (TA) proteins, bearing a C-terminal hydrophobic domain that is essential for their membrane integration. Recently, the Guided Entry of Tail-anchored proteins (GET) pathway was described in mammalian and yeast cells that serve as a blueprint of TA protein insertion [Schuldiner M, et al. (2008) *Cell* 134(4):634–645; Stefanovic S, Hegde RS (2007) *Cell* 128(6):1147–1159]. This pathway consists of six proteins, with the cytosolic ATPase GET3 chaperoning the newly synthesized TA protein posttranslationally from the ribosome to the endoplasmic reticulum (ER) membrane. Structural and biochemical insights confirmed the potential of pathway components to facilitate membrane insertion, but the physiological significance in multicellular organisms remains to be resolved. Our phylogenetic analysis of 37 GET3 orthologs from 18 different species revealed the presence of two different GET3 clades. We identified and analyzed GET pathway components in *Arabidopsis thaliana* and found reduced root hair elongation in *Atget* lines, possibly as a result of reduced SNARE biogenesis. Overexpression of *At*GET3a in a receptor knockout (KO) results in severe growth defects, suggesting presence of alternative insertion pathways while highlighting an intricate involvement for the GET pathway in cellular homeostasis of plants.

GET pathway | TA proteins | SNAREs | ER membrane | root hairs

Plants show remarkable acclimation and resilience to a broad spectrum of environmental influences as a consequence of their sedentary lifestyle. On the cellular level, such flexibility requires genetic buffering capacity as well as fine-tuned signaling and response systems. Soluble *N*-ethylmaleimide–sensitive factor attachment protein receptor (SNARE) proteins make a critical contribution toward acclimation (1, 2). Their canonical function facilitates membrane fusion through tight interaction of cognate SNARE partners at vesicle and target membranes (3). This vital process guarantees cellular expansion through addition of membrane material, cell plate formation, and cargo delivery (4, 5). SNARE proteins are also involved in regulating potassium channels and aquaporins (6–8).

Most SNARE proteins are Type II oriented and referred to as tail-anchored (TA) proteins with a cytosolic N terminus and a single C-terminal transmembrane domain (TMD) (9). TA proteins are involved in vital cellular processes in all domains of life, such as chaperoning, ubiquitination, signaling, trafficking, and transcript regulation (10–13). The nascent protein is almost fully translated when the hydrophobic TMD emerges from the ribosome, requiring shielding from the aqueous cytosol to guarantee protein stability, efficient folding, and function (14). One way of facilitating this posttranslational insertion is by proteinaceous components of a Guided Entry of Tail-anchored proteins (GET) pathway that was identified in yeast and mammals (15, 16).

In yeast, recognition of nascent TA proteins is accomplished through a tripartite pretargeting complex at the ribosome consisting of SGT2, GET5, and GET4. This complex binds to the TMD and delivers the TA protein to the cytosolic ATPase GET3 (17, 18). GET3 arranges as zinc-coordinating homodimer and shuttles the client protein to the endoplasmic reticulum (ER) membrane receptors GET1 and GET2, which finalize insertion of the TA protein (15, 19, 20).

This GET pathway is thought to be the main route for TA protein insertion into the ER, but surprisingly, its loss in yeast is only conditionally lethal (15). Conversely, lack of the mammalian GET3 orthologs TRC40 (transmembrane domain recognition complex of 40 kDa) leads to embryo lethality in mice, complicating global physiological analyses (21). Nevertheless, a handful of recent studies have started to analyze individual physiological consequences of the GET pathway in vivo using tissue-specific knockout (KO) approaches and observed that its function is required for a diverse range of physiological processes, such as insulin secretion, auditory perception, and photoreceptor function, in animals (22–24). A high degree of evolutionary conservation is often assumed, and it has been recognized that some components of the GET pathway are present in *Arabidopsis thaliana* (25, 26). However, considering the specific physiological roles of the GET pathway observed in yeast and mammals, its significance cannot

Significance

Root hairs are unicellular extensions of the rhizodermis, providing anchorage and an increase in surface area for nutrient and water uptake. Their fast, tip-focused growth showcases root hairs as an excellent genetic model to study physiological and developmental processes on the cellular level. We uncovered a root hair phenotype that is dependent on putative *Arabidopsis* orthologs of the Guided Entry of Tail-anchored (TA) proteins (GET) pathway, which facilitates membrane insertion of TA proteins in yeast and mammals. We found that plants have evolved multiple paralogs of specific GET pathway components, albeit in a compartment-specific manner. In addition, we show that differential expression of pathway components causes pleiotropic growth defects, suggesting alternative pathways for TA insertion and additional functions of GET in plants.

Author contributions: S.X. and C.G. designed research; S.X., D.G.M., N.W., L.Y.A., R.K., A.V., P.D., V.A.F.S., M.S., Y.-D.S., G.G., and C.G. performed research; S.X., D.G.M., M.S., Y.-D.S., G.G., and C.G. analyzed data; and C.G. wrote the paper with input from M.S.

The authors declare no conflict of interest.

This article is a PNAS Direct Submission.

Freely available online through the PNAS open access option.

See Commentary on page 1762.

[1]To whom correspondence should be addressed. Email: christopher.grefen@zmbp.uni-tuebingen.de.

This article contains supporting information online at www.pnas.org/lookup/suppl/doi:10.1073/pnas.1619525114/-/DCSupplemental.

be straightforwardly extrapolated across eukaryotes. A global genetic dissection of the pathway in a multicellular organism, let alone in plants, is currently lacking.

GET3/TRC40 are distant paralogs of the prokaryotic ArsA (arsenite-translocating ATPase), a protein that is part of the arsenic detoxification pathway in bacteria (27). Evidence points toward the GET pathway—albeit at a simpler scale—that exists already in Archaebacteria (10, 28). Because yeast and mammals are closely related in the supergroup of Opisthokonts (29), limiting any comparative power, we aimed to investigate pathway conservation in other eukaryotes. We also wanted to understand the impact that lack of GET pathway function has on plant development, considering that it started entering the textbooks as a default route for TA protein insertion.

Our results show that loss of GET pathway function in *A. thaliana* impacts on root hair length. This phenotype coincides with reduced protein levels at the plasma membrane of an important root hair-specific SNARE, conforming to the role of the GET pathway in TA protein insertion. However, similarly to yeast, no global pleiotropic phenotypes were observed, pointing to the existence of functional backup. However, ectopic overexpression of the cytosolic ATPase *At*GET3a in the putative receptor KO *Atget1* leads to severe growth defects, underscoring pathway conservation while implying an intricate role of the GET pathway in cellular homeostasis of plants.

Results

GET3 Paralogs Might Have Evolved as Early as Archaea. To identify potential orthologs of GET candidates, we used in silico sequence comparison (BLASTp and National Center for Biotechnology Information) of yeast and human GET proteins against the proteome of 16 different species from 13 phyla (Tables 1 and 2). Candidate sequences were assembled in a phylogenetic tree that, surprisingly, reveals that two distinct GET3 clades, which we

Table 1. Accession numbers of GET3/TRC40/ArsA orthologs of clade a used for the phylogenetic tree in Fig. 1 and their putative GET1/WRB and GET4/TRC40 orthologs identified via BLASTp search

	GET3/TRC40 orthologs		Up-/downstream orthologs	
Phylum and species	Accession no.	Length (aa)	GET1/WRB	GET4/TRC35
Eubacteria				
Proteobacteria				
Escherichia coli	KZO75668	583*	Not found	Not found
Proteoarchaeota				
Lokiarchaeota				
Lokiarchaeum sp.	KKK44956	338	Not found	Not found
Opisthokonta				
Chordata				
Homo sapiens	NP_004308	348	NP_004618	NP_057033
Ascomycota				
Saccharomyces cerevisiae	AAT93183	354	NP_011495	NP_014807
Amoebozoa				
Discosea				
Acanthamoeba castellanii	XP_004368068	330	XP_004353131	XP_004367722
Mycetozoa				
Dictyostelium purpureum	XP_003289495	330	Not found	XP_003283186
Archaeplastida				
Angiospermae				
Arabidopsis thaliana	NP_563640	353	NP_567498	NP_201127
Medicago truncatula	XP_013444959	358	XP_003629131	XP_003591984
Brachypodium distachyon	XP_003578462	363	XP_003564144	XP_003569076
Amborella trichopoda	XP_006857946	353	XP_006855737	ERM96291
Lycopodiophyta				
Selaginella moellendorffii	XP_002973461	360	Not found	XP_002969945 XP_002981415
Marchantiophyta				
Marchantia polymorpha	OAE26618	370	OAE20217	OAE20690
Bryophyta				
Physcomitrella patens	XP_001758936	365	XP_001760426	XP_001760372
	XP_001774198	365		XP_001758146
Chlorophyta				
Chlamydomonas reinhardtii	XP_001693332	319	XP_001695038	XP_001695333
Rhodophyta				
Galdieria sulphuraria	XP_005708637	706*	XP_005707118	XP_005704684
SAR				
Chromerida				
Vitrella brassicaformis	CEM03518	412	Not found	CEL97893
Heterokontophyta				
Nannochloropsis gaditana	EWM27451	370	EWM21897	EWM27335
Chromalveolata				
Cryptophyta				
Guillardia theta	XP_005837457	310	XP_005829401	XP_005841994

*Tandem GET3.

termed GET3a and GET3bc, respectively, exist in Archaeplastida and SAR (supergroup of stramenopiles, alveolates, and Rhizaria) but do not exist in Opisthokonts (yeast and animals) and Amoebozoa. The deep branching of the tree implies that duplication events must have occurred early in the evolution of eukaryotes (Fig. 1*A*). Interestingly, the recently identified phylum of *Lokiarchaeota*, which is thought to form a monophyletic group with eukaryotes (30), expresses two distinct GET3 orthologs, one of which aligns within the GET3bc clade while lacking some of the important sequence features of eukaryotic GET3 (Fig. S1*A*). This observation suggests that the last eukaryotic common ancestor had already acquired two copies of GET3.

In Rhodophytes and higher Angiospermae, a third GET3bc paralog branched off. Interestingly, the tandem ATPase motif—likely a consequence of gene duplication in the prokaryotic ArsA and suggested to be a key difference between ArsA and GET3/TRC40 homologs (28)—is not found in either of two *Lokiarchaeota* GET3; conversely, in Rhodophytes and SAR species, GET3 paralogs exist that contain duplications (Tables 1 and 2). Importantly, such repeats are not restricted to the GET3bc clade but also, are found among red algae GET3a orthologs (e.g., XP_005708637). Comparing sequence conservation of GET3 orthologs reveals that residues important for ATPase function are maintained in all candidates (Fig. S1 *A* and *B*). However, the sites for GET1 binding and the methionine-rich GET3 motif (31, 32) are only conserved in GET3a candidates of eukaryotes, concurring with the presence of GET1 and GET4 orthologs in most of these species (Table 1).

Strikingly, in silico analysis of the N termini of the identified GET3 orthologs predicts for almost all GET3bc—but not for GET3a candidates—the presence of a transit peptide for mitochondrial or chloroplastic import (Table 2). This observation is also in line with the fact that GET3bc proteins are, on average, larger than their GET3a paralogs (Tables 1 and 2), matching the length range of targeting sequences for the bioenergetic organelles.

Distinct Differences in Subcellular Localization of AtGET3 Paralogs. The three GET3 paralogs of *A. thaliana* were in silico-predicted to localize to the cytosol (*At*GET3a; At1g01910), chloroplast (*At*GET3b; At3g10350), and mitochondria (*At*GET3c; At5g60730), respectively (Tables 1 and 2). To corroborate these predictions, stably transformed, *A. thaliana Ubiquitin10* promoter (P_{UBQ10})-driven GFP fusions were generated (33). Confocal laser scanning microscopy (CLSM) and transmission electron microscopy (TEM)

Table 2. Accession numbers of GET3/TRC40/ArsA orthologs of clade bc used for the phylogenetic tree in Fig. 1 and their in silico prediction of an N-terminal signal/transit peptide using three different prediction tools (TargetP 1.1, ChloroP 1.1, and Predotar v1.03)

	GET3/TRC40 orthologs		Signal/transit peptide prediction		
Phylum and species	Accession no.	Length (aa)	TargetP 1.1	ChloroP 1.1	Predotar v1.03
Eubacteria					
Proteobacteria					
Escherichia coli	KZO75668	583*		Non-Eukaryote	
Proteoarchaeota					
Lokiarchaeota					
Lokiarchaeum sp.	KKK42590	329		Non-Eukaryote	
Archaeplastida					
Angiospermae					
A. thaliana	NP_187646	433	C	C	C
	NP_200881	391	M	C	M
Medicago truncatula	XP_003591867	406	C	C	Possibly C
	XP_013455984	381	C	C	C
Brachypodium distachyon	XP_003570659	403	M	C	M
	XP_010239988	371	M	—	M
Amborella trichopoda	XP_006827440	407	C	C	C
Lycopodiophyta					
Selaginella moellendorffii	XP_002974288	432	C	C	Possibly M
Marchantiophyta					
Marchantia polymorpha	OAE21403	432	C	—	C
Bryophyta					
Physcomitrella patens	XP_001781368	331	M	C	Possibly M
	XP_001764873	359		N terminus incomplete	
Chlorophyta					
Chlamydomonas reinhardtii	XP_001702275	513†	M	C	C
Rhodophyta					
Galdieria sulphuraria	XP_005705663	481	—	—	Possibly ER
	XP_005703923	757*	M	C	Possibly C
SAR					
Heterokontophyta					
Nannochloropsis gaditana	EWM30283	817*	M	—	Possibly C
Chromerida					
Vitrella brassicaformis	CEM11669	809*	M	—	Possibly ER
Chromalveolata					
Cryptophyta					
Guillardia theta	XP_005822752	418	S	C	ER

C, chloroplast; M, mitochondrion; S, signal peptide.
*Tandem GET3.
†Second P-loop motif at C terminus of protein.

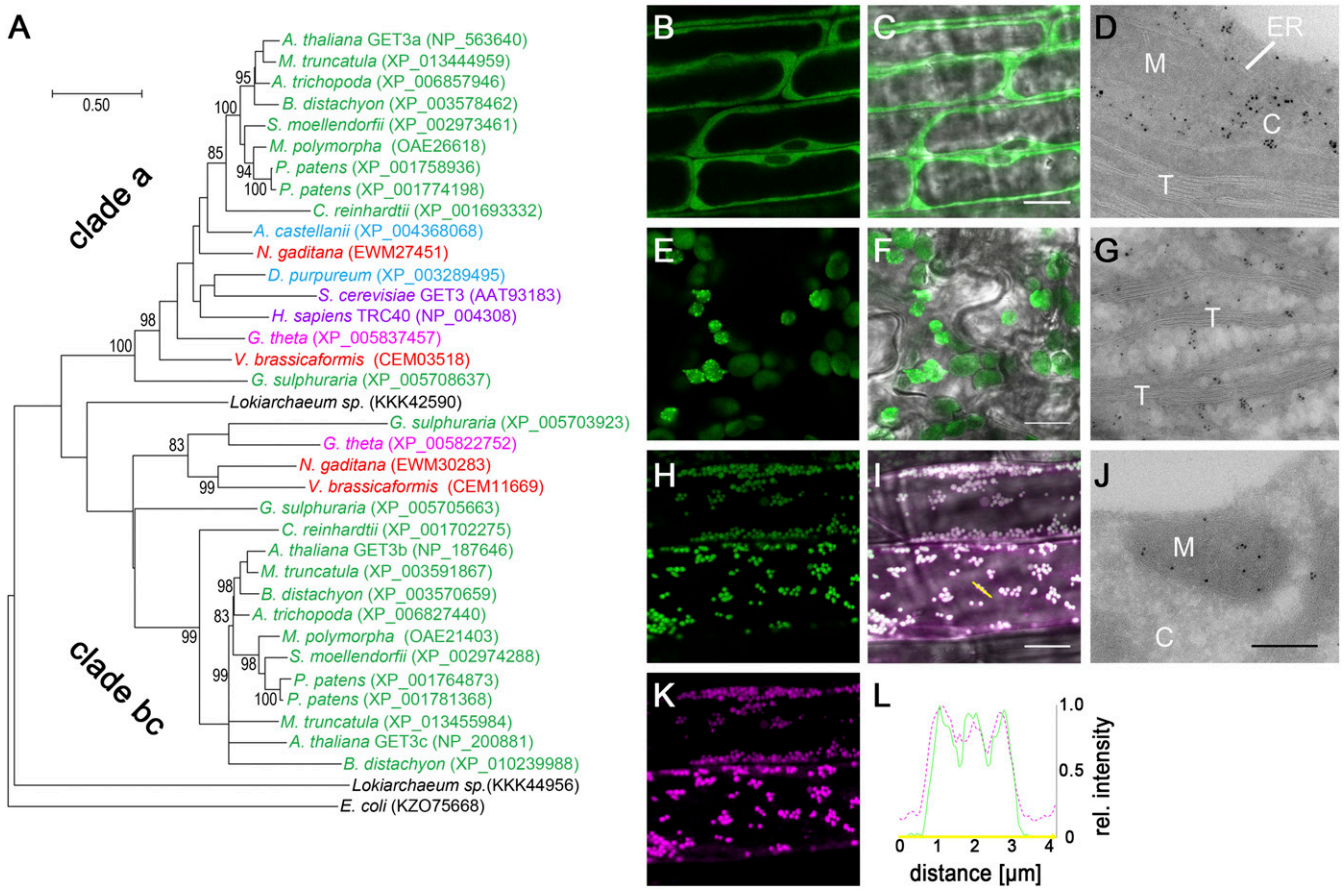

Fig. 1. Analysis of GET3 orthologs of different species. (*A*) Maximum likelihood rooted phylogenetic tree of GET3 orthologs revealing two major GET3 branches; 1,000 bootstraps were applied, and confidence ratios above 70 are included at nodes. Species color code: black, Eubacteria/Proteoarchaeota; purple, Opisthokonta; light blue, Amoebozoa; green, Archaeplastida; red, SAR; magenta, Chromalveolata. (Scale bar: changes per residue.) (*B–L*) Subcellular localization of (*B–D*) *At*GET3a, (*E–G*) *At*GET3b, and (*H–L*) *At*GET3c in stably transformed *A. thaliana* using CLSM and TEM analysis (controls in Fig. S2). (*K*) *At*GET3c-GFP–expressing specimens were treated with MitoTracker Orange to counterstain mitochondria. (*L*) Line histogram in (*I*) merged image along the yellow arrow confirms colocalization. C, cytosol; M, mitochondrion; T, thylakoid. (Scale bars: *B*, *C*, *E*, *F*, *H*, *I*, and *K*, 10 μm; *D*, *G*, and *J*, 300 nm.)

analyses reveal distinct subcellular localization patterns for three *At*GET3 paralogs (Fig. 1 *B–L* and Fig. S2): *At*GET3a is detected in the cytosol, *At*GET3b localizes to chloroplasts, and *At*GET3c localizes to mitochondria.

To resolve subplastidic localization of *At*GET3b-GFP and *At*GET3c-GFP, we used TEM analysis. Immunogold labeling indicates that *At*GET3b localizes to the stroma of chloroplasts (Fig. 1*G* and Fig. S2 *C* and *D*) and that *At*GET3c localizes to the matrix of mitochondria (Fig. 1*J* and Fig. S2 *E–G*). The mitochondrial localization of *At*GET3c had previously been reported in transiently transformed *A. thaliana* cell culture to localize to the outer mitochondrial membrane (26). By contrast, the immunogold data and high-resolution CLSM colocalization analysis of stably transformed *A. thaliana* seedlings using MitoTracker Orange consistently suggest a matrix localization for *At*GET3c (Fig. 1 *H–L*). These results are also in compliance with the presence of a transit peptide, a hallmark of organellar import (34).

Identifying the Membrane Receptor for *At*GET3a. Previous analyses have indicated that the *Sc*GET1 ortholog is missing in plants (26). Refining search parameters and using *Hs*WRB (tryptophan-rich basic protein) as template, we identified At4g16444 of *A. thaliana*. Sequence conservation of GET1 orthologs seems weaker than among GET3 candidates, but comparing TMD prediction using TMHMM (www.cbs.dtu.dk/services/TMHMM/) reveals striking structural similarity between the orthologs of different species (Fig. S1*C*). All GET1 candidates that we identified are predicted to have the typical three TMD structures of GET1/WRB with a luminal N terminus and a cytosolic C terminus as well as a cytosolic coiled coil domain between first and second TMDs (35). Additionally, publicly available microarray data confirm constitutive and well-correlated expression pattern for the putative *At*GET1 and *At*GET3a in accordance with a potential housekeeping function of the candidates (Fig. S3*D*).

To experimentally validate At4g16444 as *At*GET1, we devised localization and interaction studies. CLSM analysis of *A. thaliana* leaves that stably coexpress an ER marker protein [secreted red fluorescent protein (secRFP-HDEL)] and P_{UBQ10}-driven, C-terminally GFP-tagged *At*GET1 showed a high degree of colocalization (Fig. 2 *A–D*). Because both *Sc*GET1 and *Hs*WRB also localize to the ER membrane, this lends further support for At4g16444 being the *A. thaliana* GET1 ortholog (20, 35). Additionally, direct in planta interaction analysis using coimmunoprecipitation mass spectrometry (CoIP-MS) of *At*GET3a-GFP–expressing lines identified At4g16444 with high confidence consistently in two biological replicates among the interactors (Dataset S1).

To test interaction between *At*GET1 and all three different *At*GET3 paralogs, we used the mating-based Split-Ubiquitin System (SUS) (36). The putative *At*GET1 forms homodimers with a C-terminally tagged NubA fusion and interacts with *At*GET3a (tagged at either termini) but does not interact with the organellar localized *At*GET3b or *At*GET3c (Fig. S3*C*). Even when an N-terminal NubG tag presumably masks the transit peptides, which

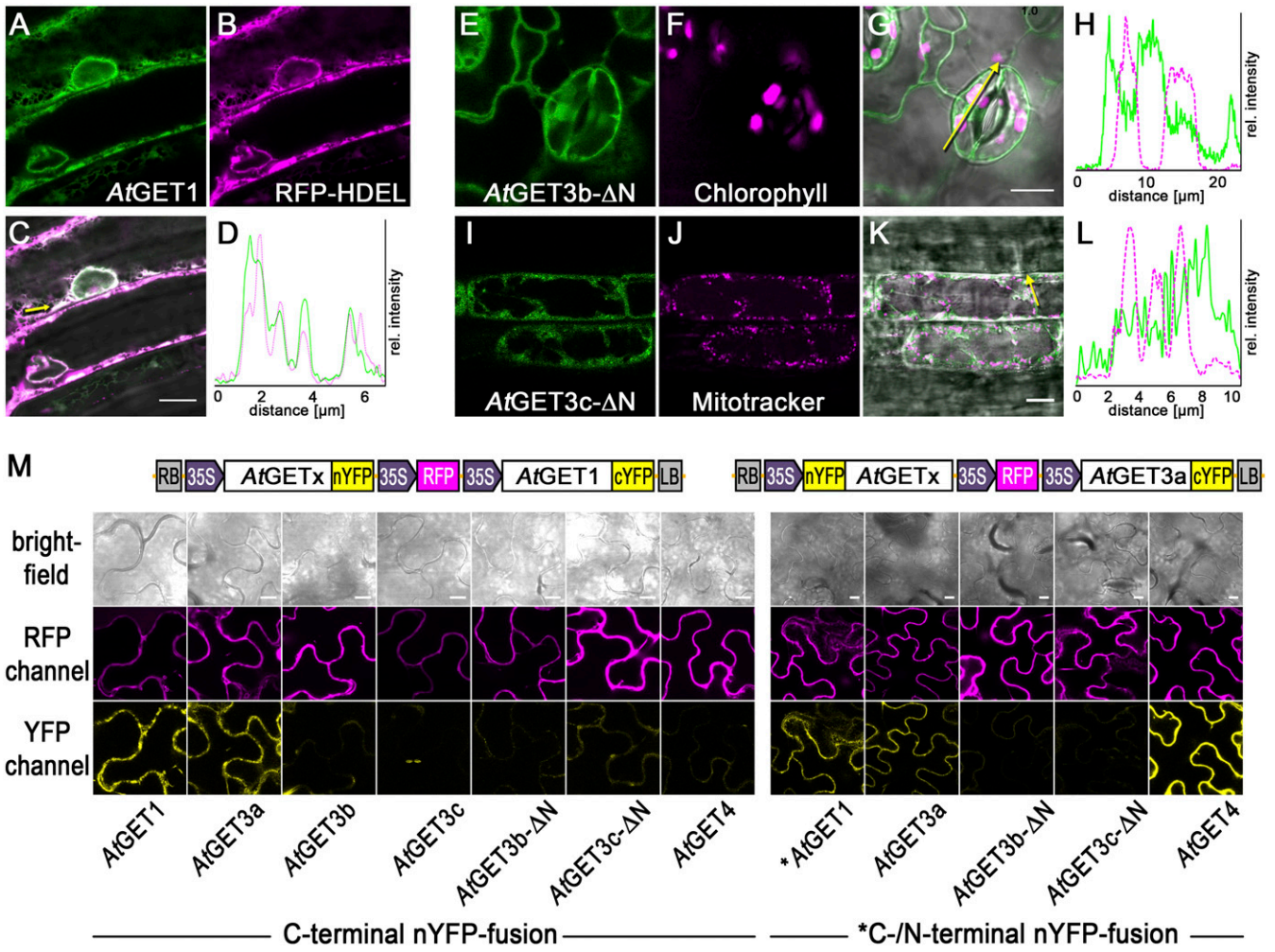

Fig. 2. Interaction analysis among *A. thaliana* GET pathway orthologs. (*A–D*) At4g16444, the putative *At*GET1, C-terminally tagged with GFP in stably transformed *A. thaliana* coexpressing the ER marker RFP-HDEL. (*D*) Line histograms along yellow arrows in *C* confirm colocalization. (*E–L*) CLSM analysis of N-terminally truncated *At*GET3b and *At*GET3c candidates. Counterimaging using autofluorescence of (*F*) chlorophyll or (*J*) MitoTracker Orange allows (*H* and *L*) line histograms in (*G* and *K*) merged images along yellow arrows that corroborate cytosolic retention. (*M*) Exemplary confocal images of rBiFC analysis of (*Left*) *At*GET1 and (*Right*) *At*GET3a with GET pathway orthologs and truncated constructs. Boxed cartoons show construct design above exemplary images of transiently transformed *Nicotiana benthamiana* leaves. A statistical analysis of the data is in Fig. S3. (Scale bars: 10 µm.)

might prevent organellar import and cause their cytosolic retention, an interaction with *At*GET1 cannot be observed.

To understand whether the physical separation of *At*GET3b/c prevents interaction with *At*GET1, we truncated the first 68 aa of *At*GET3b and 50 aa of *At*GET3c, which lead to their cytosolic localization (Fig. 2 *E–L*). We applied ratiometric bimolecular fluorescence complementation (rBiFC) (37) to assess whether such artificial mislocalization renders *At*GET3b/c susceptible to interaction with *At*GET1. Clearly, *At*GET1 homodimerizes and interacts with the cytosolic *At*GET3a but does not homodimerize or interact with the plastidic *At*GET3 paralogs or their transit peptide deletion versions (Fig. 2*M* and Fig. S3 *A* and *B*), confirming that a change in localization does not alter binding behavior. This absence of interaction seems consistent with the lack of a GET1-binding motif (32, 38) in the sequences of *At*GET3b/c, further indicating that these likely lack functional redundancy with *At*GET3a.

To test this hypothesis before phenotypic complementation, we assessed heterodimerization with *At*GET3a. Here, we also included the putative upstream binding partner of *At*GET3a, *At*GET4 (At5g63220), which we identified through in silico analysis. The expression pattern of *At*GET4 resembles that of *At*GET3a (Fig. S3*E*), and the protein localizes to the cytosol (see Fig. S7*B*). rBiFC analysis substantiates that *At*GET3a interacts with *At*GET1, itself, and *At*GET4 but fails to heterodimerize with *At*GET3b/c. Both proteins were expressed in their truncated, cytosolic form; hence, the lack of interaction cannot be attributed to compartmentalization (Fig. 2*M* and Fig. S3 *A* and *B*). Because dimerization of *Sc*GET3 is a prerequisite for function (31), this result also negates functional redundancy between GET3 paralogs.

Functional Analyses of *A. thaliana* GET Orthologs. Loss of function of TRC40, the GET3 ortholog in mammals, causes embryonic lethality befitting of the vital function of TA protein insertion (21). How would loss of GET pathway orthologs impact on survival, growth, and development in plants?

Unexpectedly, multiple different alleles of T-DNA (transfer DNA) insertion lines of each of the five *At*GET orthologs identified (Fig. S4 *A* and *B*) did not reveal any obvious growth defects. Seeds germinated, and seedlings developed indistinguishable from wild-type (WT) plants. However, a more detailed phenotypic inspection revealed that seedlings of *Atget1*, *Atget3a*, and *Atget4* lines had significantly shorter root hairs compared with Columbia-0 (Col-0) WT plants, whereas *Atget3b* and *Atget3c* did not (Fig. 3 *A* and *B* and Fig. S4*C*). Expressing genomic versions of the GET genes restores near WT-like root hair growth. By contrast, a point

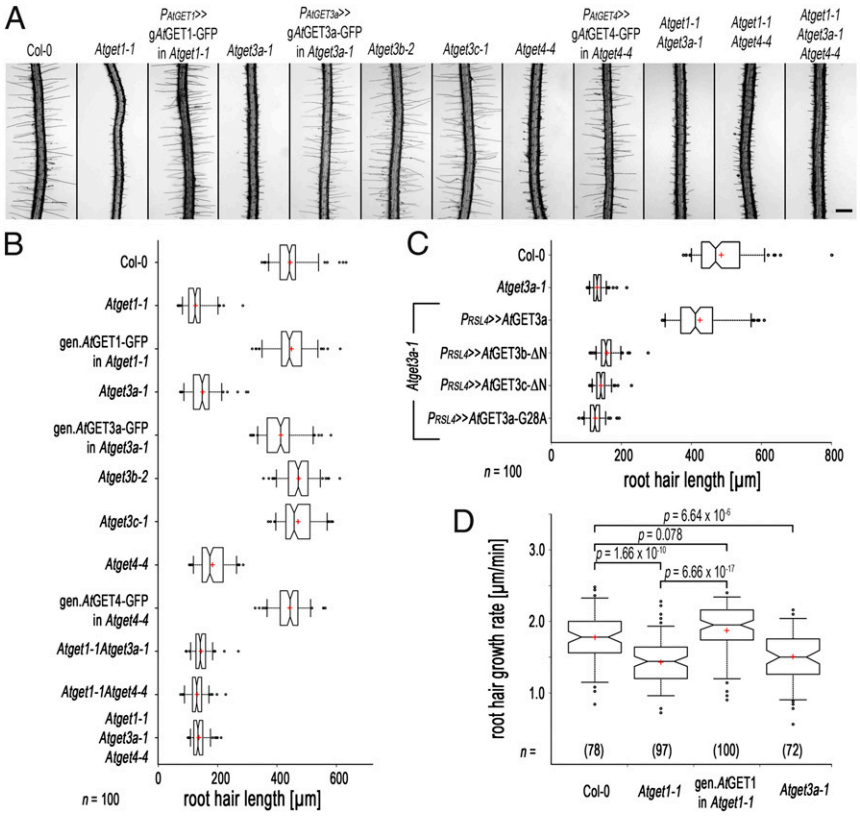

Fig. 3. Loss of function of some *A. thaliana* GET orthologs causes root hair growth defects. (*A*) Exemplary images of root elongation zones of 10-d-old T-DNA insertion lines of *A. thaliana* GET orthologs and genomic complementation. *Atget1-1*, *Atge3a-1*, and *Atget4-4* but not *Atget3b-2* and *Atget3c-1* lines show reduced growth of root hairs compared with WT Col-0 and can be complemented by their respective genomic constructs. Double or triple KOs phenocopy single T-DNA insertion lines. Transcript analysis and additional alleles can be found in Fig. S4. (*B*) Boxplot depicting length of the 10 longest root hairs of 10 individual roots ($n = 100$). Center lines of boxes represent median with outer limits at 25th and 75th percentiles. Notches indicate 95% confidence intervals; Altman whiskers extend to 5th and 95th percentiles, outliers are depicted as black dots, and red crosses mark sample means. (Scale bars: 500 µm.) (*C*) Boxplot as before, showing root hair length of Col-0 and *Atget3a-1* and complementation thereof using a root hair-specific promoter (RSL4; At1g27740) and N-terminally 3xHA-tagged coding sequences of *At*GET3a, *At*GET3b-ΔN, *At*GET3c-ΔN, and *At*GET3a-G28Ay. (*D*) Boxplot as before, showing root hair growth rates of exemplary T-DNA insertion lines and complemented *Atget1-1* line in micrometers per minute.

mutant of the P loop of the ATPase motif (*At*GET3a-G28A) expressed under a root hair-specific promoter (*RSL4*) (39) prevents rescue in *Atget3a*, suggesting that ATPase activity of *At*GET3a is essential for normal root hair growth (Fig. 3*C*). To substantiate our analysis of the *At*GET3b/c paralogs, we expressed the transit peptide deletion variants in the *Atget3a* background. The mislocalized *At*GET3b/c constructs failed to rescue the growth defects, suggesting evolution of alternative functions in the bioenergetic organelles (Fig. 3*C*).

Multiple crosses between individual T-DNA insertion lines of *At*GET1, *At*GET3a, and *At*GET4 did not yield an enhanced phenotype (i.e., further reduction of root hair length compared with their corresponding parental single-KO lines) (Fig. 3 *A* and *B*), indicating interdependent functionality of all three proteins within a joint pathway. A more detailed kinetic analysis on roots grown in RootChips (40) revealed that the shorter overall root hair length in *Atget1* and *Atget3a* correlates with slowed down growth speed (Fig. 3*D*).

Root hairs together with pollen tubes are the fastest growing cells in plants and rely on efficient delivery of membrane material to the tip (41). Although we had not observed aberrant segregation ratios of T-DNA insertion lines, which could indicate compromised fertility, we analyzed pollen tube growth in vivo and in vitro but found growth speed as well as final length unaffected in the GET pathway mutants (Fig. S4 *D* and *E*).

The genetic evidence for function of *At*GET1 and *At*GET3a in a joint pathway allowing effective root hair growth in *A. thaliana* prompted us to assess their functional conservation. In yeast, *Sc*GET1 and *Sc*GET3 are not essential; however, their absence leads to lethality under a range of different abiotic stress conditions (15). We, therefore, tested *A. thaliana* GET orthologs in BY4741 WT and corresponding KO strains for their ability to rescue yeast survival under restrictive conditions. *At*GET1 (Fig. S5*A*) and to a much lesser extent, *At*GET3a (Fig. S5*B*) hardly rescue growth in corresponding KOs, and all other *At*GET3 orthologs—full length or truncated—failed to rescue at all. This result provides strong evidence that the functions of *AtGET1* and *AtGET3a* may have diverged from yeast, more strongly so for *At*GET3a.

Loss of the GET Pathway Leads to Reduced Protein Levels of SYP123 in Root Hairs. We compared the predicted "TA-proteome" of *A. thaliana* (13) with the list of interaction partners of *At*GET3a-GFP from CoIP-MS analysis (Dataset S1). Only 23 TA proteins were detected that coprecipitated with *At*GET3a-GFP but not GFP alone (Fig. S6*B*). However, in SUS and rBiFC analysis, *At*GET3a interacts with a number of candidate TA proteins that we did not find in our CoIP-MS. Among others, the SNARE syntaxin of plants 123 (SYP123) as well as its R-SNARE partner VAMP721 and the TA protein SEC61β, subunit of the SEC61 translocon, interact with both *At*GET1 and *At*GET3a (Fig. 4*A* and Fig. S6 *A* and *C*). The SNARE SYP43 as well as the non-TA SNARE protein SNAP33 failed to interact. SYP123 is a plasma membrane-localized Qa-SNARE that specifically expresses in root hair cells, and its loss results in short root hairs (42). We crossed GFP-SYP123 under its own promoter (42) with our *Atget1-1* and *Atget3a-1* lines to analyze for misinsertion, mislocalization, or cytosolic retention.

CLSM analysis of root hairs expressing SYP123 in WT and mutant backgrounds showed normal distribution of SYP123 in bulge formation and developed root hairs (Fig. S7*A*). No cytosolic aggregates or increased fluorescence foci were visible in the cytoplasm, which was reminiscent of findings in yeast *get* pathway KOs (15, 43). However, we repeatedly observed differences in GFP signal under identical conditions and settings. GFP fluorescence intensity of root hairs is consistently stronger in the WT than in *Atget1* and *Atget3a* lines (Fig. 4*B*), suggestive of lower SYP123 protein levels in the plasma membrane of *Atget* lines.

To substantiate this finding, we performed membrane fractionation of protein extracts from roughly 250 roots per line (Fig. 4*C*). Immunoblot analysis revealed that GFP-SYP123 levels in the membrane fraction of *Atget1* and *Atget3a* lines were strikingly lower than in WT background, suggesting that loss of GET pathway functionality reduces SYP123 abundance

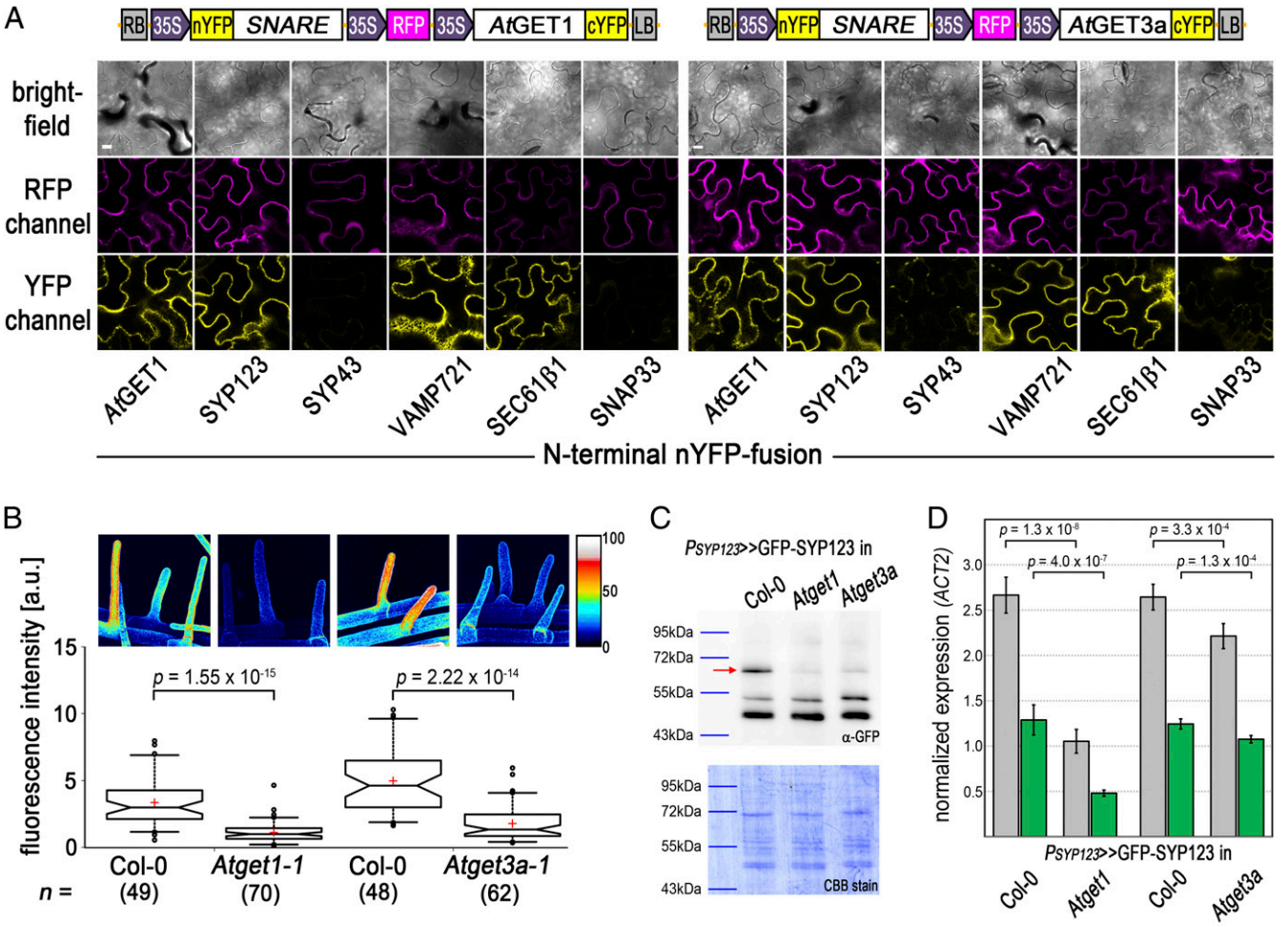

Fig. 4. The root hair-specific Qa-SNARE SYP123 shows reduced protein levels in *Atget* lines. (*A*) rBiFC analysis of (*Left*) AtGET1 and (*Right*) AtGET3a with candidate SNARE/TA proteins. Boxed cartoons show construct design above representative images of epidermal cells from transiently transformed *N. benthamiana* leaves. The statistical analysis of the data is presented in Fig. S6C. (Scale bars: 10 μm.) (*B* and *C*) Analysis of root hairs expressing P_{SYP123} >> GFP-SYP123 in *Atget1*-1, *Atget3a*-1, or corresponding Col-0 WT. (*B*) Boxplot of root hair fluorescence intensities of average-intensity *z* projections (number in parentheses below the *x* axis). Boxplot as in Fig. 3; *P* values confirm a significant difference in fluorescence intensity between GFP-SYP123 expression in WT (stronger) vs. T-DNA insertion lines (weaker). Heat maps of exemplary *z* projections are in *Upper*. (*C*) Anti-GFP immunoblots of membrane fractions from the marker lines detect a strong GFP-SYP123 band at 62.8 kDa, which is significantly and visibly weaker in *Atget3a* and *Atget1* lines than in WT Col-0. Bands below are likely the result of unspecific cross-reaction of antibody and plant extract. Coomassie brilliant blue staining (CBB stain) of blot confirms equal loading of protein. (*D*) qRT-PCR analysis of SYP123 transcript levels was performed using either SYP123- (gray) or GFP-specific (green) primers to resolve differences in mRNA levels on Col-0, *Atget1*, or *Atget3a* background. Expression levels were normalized to the Actin2 control. Error bars: SD ($n = 6$).

in the membrane. Quantitative RT-PCR (qRT-PCR) analyses further indicated that SYP123 transcript levels are also reduced in both mutants compared with the WT, with a milder transcript reduction in the *Atget3a* than in the *Atget1* background (Fig. 4*D*). Notably, the differences between endogenous and transgenic levels of transcript remain equal in all lines at roughly 50%, which confirms native expression of the marker construct (44) and suggests regulation of SYP123 in *get* lines also at transcript level.

Overexpression of *At*GET3a in *Atget1* Reveals Severe Growth Defects. The general viability of *Atget* mutants and the fact that at least part of SYP123 finds its way to the plasma membrane in root hairs of mutants question the role of the GET pathway as the sole route for TA protein insertion in *A. thaliana*. To further understand the physiological importance of the pathway in planta, we crossed the overexpressing *At*GET3a-GFP with the *Atget1-1* line. The rationale was to synthetically increase the activity of an upstream player, while limiting downstream capacity of the pathway to enhance phenotypes associated with dysfunction of the pathway. Such overexpression of the cytosolic *At*GET3a in its receptor KO leads to dwarfed plants. Main inflorescence, root, silique, and seed development are severely compromised compared with the parental lines (Fig. 5 *A–C* and Fig. S7 *C–F*). In addition to the obvious aboveground phenotype, the growth of root hairs is impaired more strongly compared with the individual loss of function *Atget1-1* lines (Fig. S7*F*). Such stronger phenotype might be a consequence of short-circuiting alternative insertion pathways, further depleting vital TA proteins from reaching their site of action.

CLSM analysis of the subcellular expression of *At*GET3-GFP in the leaf epidermis of homozygous *Atget1* lines reveals cells with increased GFP fluorescence in foci among cells that resemble the normal cytoplasmic distribution of *At*GET3a-GFP (Fig. 5*D*, *Right* and Movie S1). Conversely, no cells with GFP foci are present in leaf samples of heterozygous *Atget1*$^{(+/-)}$ lines expressing the same construct, and an even cytoplasmic distribution of *At*GET3a-GFP is observable instead (Fig. 5*D*, *Left* and Movie S2). Foci may be a result of clustering of uninserted TA proteins with multimers of *At*GET3a, similar to effects observed in yeast *Δget1* KOs (43, 45). We have also analyzed expression of

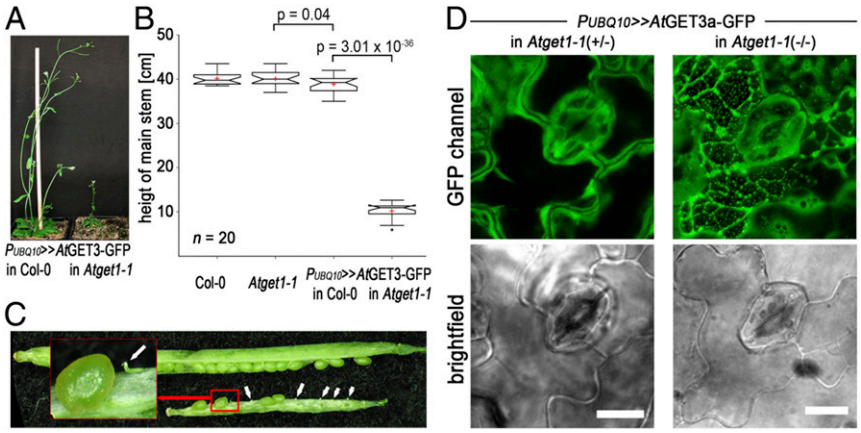

Fig. 5. Ectopic overexpression of *At*GET3a in *Atget1* causes severe growth defects. (*A*) Exemplary images of 6-wk-old *A. thaliana* plants expressing *At*GET3a-GFP in either Col-0 WT or *Atget1* showing significant differences in growth. (*B*) Boxplot summarizing the height of the main inflorescences of 20 individual 6-wk-old *A. thaliana* lines as labeled below the *x* axis. Boxplot as in Fig. 3 but with Tukey whiskers that extend to 1.5× interquartile range. (*C*) Siliques of mutant plants [*At*GET3a-GFP in *Atget1* (silique below)] show a high number of aborted embryos in contrast to single *Atget1* lines (silique above). The statistical analysis can be found in Fig. S7C. (*D*) Maximum projection *z* stacks of 20 images at 1.1-μm optical slices at 63× magnification showing subcellular localization of *At*GET3a-GFP in (*Left*) heterozygous or (*Right*) homozygous *Atget1-1* lines. Bright-field images below are taken from the 10th image in each stack. The full *z* stacks are shown in Movies S1 and S2. (Scale bars: 10 μm.)

*At*GET4-mCherry in an *Atget1-1* background but did not detect similar aggregate-like structures (Fig. S7*B*).

Discussion

Numerous biochemical and structural insights from yeast and in vitro systems have convincingly established the ability of the GET pathway to facilitate membrane insertion of TA proteins (reviewed in ref. 46). However, because TRC40 KO mice are embryonic lethal, physiological consequences of GET loss of function in an in vivo context remain insufficiently understood, and those that are available are typically specific to mammalian features. Such findings are in contrast to the high degree of conservation that GET homologs show across the eukaryotic domain, a situation where the model plant *A. thaliana* provides a highly suitable system for additional study.

Phylogenetic analysis of GET pathway components reveals an alternative GET3 clade, which must have evolved before the last eukaryotic ancestor. This hypothesis becomes apparent from the deeply branching phylogenetic tree (Fig. 1*A*) but also, by the presence of a second distinct GET3 homolog in the recently discovered *Lokiarchaeum* sp., which forms a monophyletic group with eukaryotes (30). One of the *Ls*GET3 copies aligns within the GET3bc clade, with sequences that seem to only exist in Archaeplastida and SAR, whereas Opisthokonts and Amoebozoa may have lost this paralog. GET3bc branched off once more in some red algae and higher plants to evolve another plastidic GET3 paralog. It is unlikely that this third paralog is the result of endosymbiosis, because its sequence homology is too closely related to the other organellar candidate.

Neither root hair nor general growth in *A. thaliana* seem affected by lack of *At*GET3b/c, and their biological function will require dedicated study in the future. Their localization in the plastid stroma and the mitochondrial matrix; failure to interact with *At*GET1, *At*GET3a, or *At*GET4; absence of obvious downstream candidates to facilitate membrane insertion; lack of conserved sequence motifs for TA binding (Fig. S1); and failure to complement the *At*GET3a-related growth defects (Fig. 3*C*) deem it unlikely that *At*GET3b/c function is related to TA protein insertion.

A previous structural analysis of an archaeal (*Methanocaldococcus jannaschii*) GET3 ortholog inferred some key features that would distinguish GET3 from its prokaryotic ArsA ancestor sequence (28), namely the tandem repeat (exclusive to ArsA) and a conserved CxxC motif (specific for GET3). By contrast, our phylogenetic analysis uncovered the tandem repeat in candidate sequences of both eukaryotic GET3 clades, disproving it as a decisive feature solely of ArsA. Such sequence repeats may explain the presence of a third closely related GET3 paralog in higher plants and red algae as a consequence of an earlier tandem duplication, but this hypothesis requires in-depth analysis of more sequences from different species.

The CxxC motif, which is found in both Metazoa and Fungi GET3 orthologs, also exists in the Amoebozoan and *Lokiarchaeota* GET3 orthologs and seemingly plays a role in zinc binding/coordination (19). However, this motif is absent in the Archaeplastida and SAR GET3a orthologs, where other invariant cysteines—CVC—some 40 aa upstream of the presumed CxxC motif are present. In contrast to the CxxC motif, the CVC motif can be found in all eukaryotic GET3a orthologs that we analyzed. Nevertheless, the CxxC motif is required for *Sc*GET3 to act as a general chaperone under oxidative stress conditions, binding unfolded proteins and preventing their aggregation (43, 45). Hence, it is conceivable that GET3bc paralogs—that feature CxxC (Fig. S1*B*)—have evolved as organellar chaperones with putative thiol-disulfide oxidoreductase function and lost (or never had) the TA insertion capability, whereas GET3a orthologs maintained (or acquired) both functions. Notably, the chaperone function of *Sc*GET3 is ATP-independent, whereas TA-insertase activity depends on ATP (43). A version of *At*GET3a, where the ATPase motif is mutated (G28A), fails to rescue the root hair growth phenotype (Fig. 3*C*), suggesting that it is caused by the TA insertion function of *At*GET3a, which is dependent on ATPase function (15).

Generally, T-DNA insertion in *AtGET1*, *AtGET3a*, or *AtGET4* leads to a reduction in root hair growth. Complementation with tagged or genomic constructs of the corresponding genes rescues normal growth connecting phenotype with genotype. Interestingly, multiple crosses between loss of function lines of three key players of an *A. thaliana* GET pathway do not lead to a more severe phenotype (i.e., even shorter root hairs than the single T-DNA insertion lines as measured, e.g., in plants overexpressing *At*GET3a-GFP in *Atget1*) (Fig. S7*F*). This observation indicates that the three genes act in a linear pathway in *A. thaliana*, which is in agreement with findings in other species (15, 16). Nevertheless, it seems difficult to reconcile our findings with a putative GET pathway as the sole and global route responsible for insertion of TA proteins in plants similar to its proposed role in yeast or mammals (46). Of the estimated 500 TA proteins in *A. thaliana* (13), many are vital for development and survival of the plant. Especially SNARE proteins, which facilitate vesicle fusion to drive processes, such as cytokinesis, pathogen defense, and ion homeostasis (4, 7, 47), require correct and efficient membrane insertion. Inability of the plant to insert TA proteins should yield severe growth defects at least similar to if not stronger than—for example—the *knolle* phenotype caused by an *syp111* loss of function allele (coding for the Qa-SNARE KNOLLE). *Knolle* plants fail to grow beyond early seedling stage because of incomplete cell plate formation (48).

Absence of the root hair-specific Qa-SNARE SYP123 was shown to cause defects in root hair growth (42) as a result of reduced vesicle trafficking. Although lack of *At*GET pathway components in planta did not lead to complete absence or mislocalization of SYP123 within the plasma membrane of root hairs, a significant reduction of protein levels was observed in vivo. Although this result was also confirmed biochemically, levels of SYP123 mRNA in *Atget1* as well as *Atget3a* lines are also

reduced (Fig. 4*D*), albeit not as strongly as the reduction of protein detected in the membrane fraction of mutants (Fig. 4*C*). Taken together, our findings indicate feedback control, where loss of *At*GET function and the resulting failure of SYP123 protein insertion activate inhibition at the transcript level to decrease steady-state levels of both mRNA and protein. Functional cross-talk between the GET pathway and its impact on transcript regulation had been shown previously in other eukaryotes (23, 49).

The fact that lack of GET function can phenotypically only be detected in root hairs might be associated with these requiring fast and efficient trafficking of cargo and membrane material to the tip (42). Hence, slight imbalances in protein biogenesis owing to the absence of one major insertion pathway might strain alternative but unknown insertion systems, at which point lack of the GET pathway becomes rate-limiting. This effect is not reoccurring in the other fast-growing plant cells—pollen tubes—not only suggesting presence of an alternative pathway but also, questioning the monopoly of TA protein insertion of the GET pathway. Nevertheless, our SYP123 case study supports a role of the GET pathway in planta for regulating SNARE abundance. Interaction of *At*GET1 and *At*GET3a with a wide range of different TA proteins was also shown, but we identified two TA proteins that failed to interact (SYP43 and At5g40510). Also, CoIP-MS analysis of *At*GET3a-GFP detected only about 23 TA proteins, less than 5% of all TA proteins predicted to be present in *A. thaliana* (13) (Fig. S6*B*). Although the latter might be attributed to weak or transient binding of the TMD with *At*GET3a or premature dissolution of binding through experimental conditions, it nevertheless raises questions as to the GET pathway being exclusively engaged in TA protein insertion into the ER. Among the many proteins that were detected in CoIP-MS analysis with *At*GET3a-GFP, a lot of non-TA proteins but proteins related to trafficking or proteostasis were detected (Dataset S1). If some of these interactions can be confirmed in future studies, functional analyses might uncover alternative roles for *At*GET3a.

Our findings are summarized in a working model of a presumed GET pathway in plants (Fig. 6). While under normal growth conditions, the GET pathway acts as main route for TA protein insertion into the ER membrane (Fig. 6*A*), and loss of either component or a combination thereof brings alternative pathways into play (Fig. 6*B*). The existence of alternative insertion mechanisms is indicated by not only the relatively mild phenotype but also, the limited number of TA proteins that we found to interact with *At*GET3a, raising the question of how TA proteins that do not interact with GET pathway components get inserted into membranes. In yeast, it has been shown that some TA proteins can insert unassisted and that chaperoning in the cytosol is facilitated by heatshock proteins (50); however, any alternative receptor remains elusive. Presence of an alternative insertion pathway in *A. thaliana* is also supported by the overexpression of the cytosolic *At*GET3a in its receptor KO, which has severe phenotypic consequences (Figs. 5 and 6*C*). This observation corroborates a hierarchical connection of *At*GET3a and *At*GET1, because presence of the latter can rescue the growth defects. It further suggests the existence of an alternative pathway for TA insertion with weaker affinity toward pretargeting factors, such as *At*GET4, at the ribosome, because the aberrant amounts of *At*GET3a seem to deplete the alternative pathway. Lastly, the *At*GET3a foci that can occur in cells of mutant plants (but never in the WT background) (Fig. 5*D*) and that are similar to aggregates observed in stressed yeast cells (43) suggest additional functions of *At*GET3a that nonetheless depend on *At*GET1. The aggregate-like structures were not found in all cells of mutant plants, suggesting a dosage-dependent effect (i.e., if levels of *At*GET3a-GFP exceed a certain threshold, clustering occurs). Clusters may consist of multimers of *At*GET3a, complexes of *At*GET3a bound to TA proteins, or *At*GET3a/TA proteins bound to the elusive *At*GET2 receptor. In yeast, *Sc*GET2 is the first contact point at receptor level for the *Sc*GET3-TA protein complex before the TA protein is delivered to *Sc*GET1 (20); hence, lack of *At*GET1 could keep a putative *At*GET3a/TA protein aggregate stably in the vicinity of the ER.

Future work on this mutant in particular will help to resolve functions of GET components in *A. thaliana*. A current debate about potential cross-talk between GET components in TA protein insertion and protein quality control in yeast and animal cells (51) may be further underpinned by our findings in plants, which provide the fundament to broad comparative investigations in the near future.

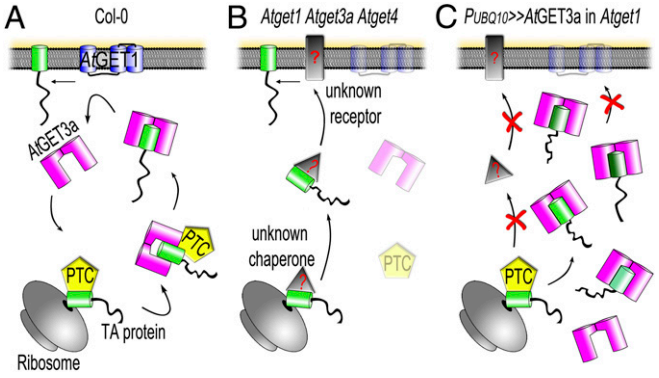

Fig. 6. Model hypothesizing the subcellular mechanism of *A. thaliana* GET orthologs. (*A*) In WT Col-0, a pretargeting complex (PTC) likely comprising *A. thaliana* SGT2 and GET5 (both of which revealed many potential orthologs through in silico analyses) as well as the in silico-identified *At*GET4, which interacts with *At*GET3a in vivo, might receive nascent TA proteins from the ribosome and deliver these to the homodimer of *At*GET3a, in turn shuttling the client TA protein to the ER receptor *At*GET1 (an *At*GET2 could not be identified through extensive BLASTp analysis and was left out of the figure). (*B*) The hypothetical situation in a single *Atget1*, *Atget3a*, or *Atget4* or crosses thereof. In the absence of a functional GET pathway, most TA proteins are delivered by an unknown alternative pathway (depicted as a gray triangle or rectangle with red question marks). (*C*) Overexpression of *At*GET3a in absence of a docking station to unload client TA proteins might lead to cytosolic aggregates and block of TA insertion. The affinity between the PTC and *At*GET3a might be a decisive factor here, because the unknown alternative pathway does not seem to compensate for the aberrant presence of *At*GET3a.

Materials and Methods

Plant Growth Conditions. Seeds were grown on 1/2 Murashige and Skoog medium including 1% sugar and 0.9% plant agar, pH 5.7. Plants were cultivated in a 16-h light/8-h dark cycle at 18 °C or 23 °C in the growth chamber (*SI Materials and Methods*).

Construct Design. Most constructs were designed by Gateway Recombination Reaction; vectors used for localization analyses can be found in ref. 33. A full list of oligonucleotides and constructs can be found in Tables S1 and S2 (*SI Materials and Methods*).

Interaction Analyses. We performed rBiFC in transiently transformed tobacco according to the work in ref. 37 (*SI Materials and Methods*).

Microscopy. CLSM microscopy was performed using a Leica SP8 at the following laser settings: GFP at 488-nm excitation (ex) and 490- to 520-nm emission (em); YFP at 514-nm ex and 520- to 560-nm em; and RFP/Mitotracker at 561-nm ex and 565- to 620-nm em. Chlorophyll autofluorescence was measured using the 488-nm laser line and em at 600–630 nm. TEM analysis and more details are in *SI Materials and Methods*.

T-DNA Lines. The following T-DNA lines were characterized (Fig. S4 *A* and *B*): Sail_1210_E07 (*Atget1-1*), GK_246D06 (*Atget1-2*), SALK_033189 (*Atget3a-1*), SALK_100424 (*Atget3a-2*), SALK_012980 (*Atget3a-3*), SALK_017702 (*Atget3b-2*), SALK_091152 (*Atget3c-1*), SALK_069782 (*Atget4-1*), and SALK_121195 (*Atget4-4*). This work suggests new names for *Arabidopsis thaliana* genes previously termed "unknown": *At*GET1 (At4g16444), *At*GET3a (At1g01910), *At*GET3b (At3g10350), *At*GET3c (At5g60730), and *At*GET4 (At5g63220).

More details and other methods are in *SI Materials and Methods*.

Note Added in Proof. During revision of this article, an analysis of conditional *wrb* KO mice demonstrated that the GET pathway is required for only a subset—but not all—TA proteins in vivo (67). Also, an alternative ER insertion pathway was described in yeast (68) and another study reported an ER-stress and early flowering phenotype of the *Atget1-1* and *Atget3a-1* lines (69).

ACKNOWLEDGMENTS. We thank Masa H. Sato for sharing the GFP-SYP123 marker line and Gabriel Schaaf for vector pDRf1-GW and yeast strains. MS analysis was done at the Proteomics Centre, University of Tübingen, and we thank Mirita Franz-Wachtel for her help in interpreting the data. We also thank Gerd Jürgens and Marja Timmermans for critical discussions and comments on the manuscript, Antje Feller and Jaquelynn Mateluna for help with the quantitative PCR analysis, and Eva Schwörzer and Laure Grefen for technical support. This work was supported by an Emmy Noether Fellowship SCHW 1719/1-1 from the Deutsche Forschungsgemeinschaft (DFG; to M.S.), CellNetworks Research Group funds (to G.G.), seed funding through the Collaborative Research Council 1101 (SFB1101; to C.G.), and an Emmy Noether Fellowship GR 4251/1-1 from the DFG (to C.G.).

1. Lipka V, Kwon C, Panstruga R (2007) SNARE-ware: The role of SNARE-domain proteins in plant biology. *Annu Rev Cell Dev Biol* 23:147–174.
2. Grefen C, Blatt MR (2008) SNAREs–molecular governors in signalling and development. *Curr Opin Plant Biol* 11(6):600–609.
3. Rizo J, Südhof TC (2012) The membrane fusion enigma: SNAREs, Sec1/Munc18 proteins, and their accomplices–guilty as charged? *Annu Rev Cell Dev Biol* 28:279–308.
4. Jürgens G, et al. (2015) Plant cytokinesis: A tale of membrane traffic and fusion. *Biochem Soc Trans* 43(1):73–78.
5. Surpin M, et al. (2003) The VTI family of SNARE proteins is necessary for plant viability and mediates different protein transport pathways. *Plant Cell* 15(12):2885–2899.
6. Hachez C, et al. (2014) Arabidopsis SNAREs SYP61 and SYP121 coordinate the trafficking of plasma membrane aquaporin PIP2;7 to modulate the cell membrane water permeability. *Plant Cell* 26(7):3132–3147.
7. Grefen C, et al. (2015) A vesicle-trafficking protein commandeers Kv channel voltage sensors for voltage-dependent secretion. *Nat Plants* 1:15108.
8. Zhang B, et al. (2015) The Arabidopsis R-SNARE VAMP721 interacts with KAT1 and KC1 K+ channels to moderate K+ current at the plasma membrane. *Plant Cell* 27(6):1697–1717.
9. Borgese N, Colombo S, Pedrazzini E (2003) The tale of tail-anchored proteins: Coming from the cytosol and looking for a membrane. *J Cell Biol* 161(6):1013–1019.
10. Borgese N, Fasana E (2011) Targeting pathways of C-tail-anchored proteins. *Biochim Biophys Acta* 1808(3):937–946.
11. Beilharz T, Egan B, Silver PA, Hofmann K, Lithgow T (2003) Bipartite signals mediate subcellular targeting of tail-anchored membrane proteins in Saccharomyces cerevisiae. *J Biol Chem* 278(10):8219–8223.
12. Kalbfleisch T, Cambon A, Wattenberg BW (2007) A bioinformatics approach to identifying tail-anchored proteins in the human genome. *Traffic* 8(12):1687–1694.
13. Kriechbaumer V, et al. (2009) Subcellular distribution of tail-anchored proteins in Arabidopsis. *Traffic* 10(12):1753–1764.
14. Hegde RS, Keenan RJ (2011) Tail-anchored membrane protein insertion into the endoplasmic reticulum. *Nat Rev Mol Cell Biol* 12(12):787–798.
15. Schuldiner M, et al. (2008) The GET complex mediates insertion of tail-anchored proteins into the ER membrane. *Cell* 134(4):634–645.
16. Stefanovic S, Hegde RS (2007) Identification of a targeting factor for posttranslational membrane protein insertion into the ER. *Cell* 128(6):1147–1159.
17. Chang YW, et al. (2010) Crystal structure of Get4-Get5 complex and its interactions with Sgt2, Get3, and Ydj1. *J Biol Chem* 285(13):9962–9970.
18. Simpson PJ, Schwappach B, Dohlman HG, Isaacson RL (2010) Structures of Get3, Get4, and Get5 provide new models for TA membrane protein targeting. *Structure* 18(8):897–902.
19. Metz J, Wächter A, Schmidt B, Bujnicki JM, Schwappach B (2006) The yeast Arr4p ATPase binds the chloride transporter Gef1p when copper is available in the cytosol. *J Biol Chem* 281(1):410–417.
20. Wang F, Chan C, Weir NR, Denic V (2014) The Get1/2 transmembrane complex is an endoplasmic-reticulum membrane protein insertase. *Nature* 512(7515):441–444.
21. Mukhopadhyay R, Ho YS, Swiatek PJ, Rosen BP, Bhattacharjee H (2006) Targeted disruption of the mouse Asna1 gene results in embryonic lethality. *FEBS Lett* 580(16):3889–3894.
22. Daniele LL, Emran F, Lobo GP, Gaivin RJ, Perkins BD (2016) Mutation of wrb, a component of the guided entry of tail-anchored protein pathway, disrupts photoreceptor synapse structure and function. *Invest Ophthalmol Vis Sci* 57(7):2942–2954.
23. Norlin S, Parekh VS, Naredi P, Edlund H (2016) Asna1/TRC40 controls β-cell function and endoplasmic reticulum homeostasis by ensuring retrograde transport. *Diabetes* 65(1):110–119.
24. Vogl C, et al. (2016) Tryptophan-rich basic protein (WRB) mediates insertion of the tail-anchored protein otoferlin and is required for hair cell exocytosis and hearing. *EMBO J* 35(23):2536–2552.
25. Abell BM, Mullen RT (2011) Tail-anchored membrane proteins: Exploring the complex diversity of tail-anchored-protein targeting in plant cells. *Plant Cell Rep* 30(2):137–151.
26. Duncan O, van der Merwe MJ, Daley DO, Whelan J (2013) The outer mitochondrial membrane in higher plants. *Trends Plant Sci* 18(4):207–217.
27. Zhou T, Radaev S, Rosen BP, Gatti DL (2000) Structure of the ArsA ATPase: The catalytic subunit of a heavy metal resistance pump. *EMBO J* 19(17):4838–4845.
28. Suloway CJ, Rome ME, Clemons WM, Jr (2012) Tail-anchor targeting by a Get3 tetramer: The structure of an archaeal homologue. *EMBO J* 31(3):707–719.
29. Adl SM, et al. (2012) The revised classification of eukaryotes. *J Eukaryot Microbiol* 59(5):429–493.
30. Spang A, et al. (2015) Complex archaea that bridge the gap between prokaryotes and eukaryotes. *Nature* 521(7551):173–179.
31. Mateja A, et al. (2009) The structural basis of tail-anchored membrane protein recognition by Get3. *Nature* 461(7262):361–366.
32. Stefer S, et al. (2011) Structural basis for tail-anchored membrane protein biogenesis by the Get3-receptor complex. *Science* 333(6043):758–762.
33. Grefen C, et al. (2010) A ubiquitin-10 promoter-based vector set for fluorescent protein tagging facilitates temporal stability and native protein distribution in transient and stable expression studies. *Plant J* 64(2):355–365.
34. Garg SG, Gould SB (2016) The role of charge in protein targeting evolution. *Trends Cell Biol* 26(12):894–905.
35. Vilardi F, Lorenz H, Dobberstein B (2011) WRB is the receptor for TRC40/Asna1-mediated insertion of tail-anchored proteins into the ER membrane. *J Cell Sci* 124(Pt 8):1301–1307.
36. Grefen C, Obrdlik P, Harter K (2009) The determination of protein-protein interactions by the mating-based split-ubiquitin system (mbSUS). *Methods Mol Biol* 479:217–233.
37. Grefen C, Blatt MR (2012) A 2in1 cloning system enables ratiometric bimolecular fluorescence complementation (rBiFC). *Biotechniques* 53(5):311–314.
38. Mariappan M, et al. (2011) The mechanism of membrane-associated steps in tail-anchored protein insertion. *Nature* 477(7362):61–66.
39. Datta S, Prescott H, Dolan L (2015) Intensity of a pulse of RSL4 transcription factor synthesis determines Arabidopsis root hair cell size. *Nat Plants* 1:15138.
40. Grossmann G, et al. (2011) The RootChip: An integrated microfluidic chip for plant science. *Plant Cell* 23(12):4234–4240.
41. Grierson C, Nielsen E, Ketelaarc T, Schiefelbein J (2014) Root hairs. *Arabidopsis Book* 12:e0172.
42. Ichikawa M, et al. (2014) Syntaxin of plant proteins SYP123 and SYP132 mediate root hair tip growth in Arabidopsis thaliana. *Plant Cell Physiol* 55(4):790–800.
43. Voth W, et al. (2014) The protein targeting factor Get3 functions as ATP-independent chaperone under oxidative stress conditions. *Mol Cell* 56(1):116–127.
44. Enami K, et al. (2009) Differential expression control and polarized distribution of plasma membrane-resident SYP1 SNAREs in Arabidopsis thaliana. *Plant Cell Physiol* 50(2):280–289.
45. Powis K, et al. (2013) Get3 is a holdase chaperone and moves to deposition sites for aggregated proteins when membrane targeting is blocked. *J Cell Sci* 126(Pt 2):473–483.
46. Denic V, Dötsch V, Sinning I (2013) Endoplasmic reticulum targeting and insertion of tail-anchored membrane proteins by the GET pathway. *Cold Spring Harb Perspect Biol* 5(8):a013334.
47. Kwon C, et al. (2008) Co-option of a default secretory pathway for plant immune responses. *Nature* 451(7180):835–840.
48. Lukowitz W, Mayer U, Jürgens G (1996) Cytokinesis in the Arabidopsis embryo involves the syntaxin-related KNOLLE gene product. *Cell* 84(1):61–71.
49. Jonikas MC, et al. (2009) Comprehensive characterization of genes required for protein folding in the endoplasmic reticulum. *Science* 323(5922):1693–1697.
50. Johnson N, Powis K, High S (2013) Post-translational translocation into the endoplasmic reticulum. *Biochim Biophys Acta* 1833(11):2403–2409.
51. Casson J, McKenna M, High S (2016) On the road to nowhere: Cross-talk between post-translational protein targeting and cytosolic quality control. *Biochem Soc Trans* 44(3):796–801.
52. Kumar S, Stecher G, Tamura K (2016) MEGA7: Molecular Evolutionary Genetics Analysis Version 7.0 for Bigger Datasets. *Mol Biol Evol* 33(7):1870–1874.
53. Karnik A, Karnik R, Grefen C (2013) SDM-Assist software to design site-directed mutagenesis primers introducing "silent" restriction sites. *BMC Bioinformatics* 14:105.
54. Xing S, Wallmeroth N, Berendzen KW, Grefen C (2016) Techniques for the analysis of protein-protein interactions in vivo. *Plant Physiol* 171(2):727–758.
55. Grefen C (2014) The split-ubiquitin system for the analysis of three-component interactions. *Methods Mol Biol* 1062:659–678.
56. Hecker A, et al. (2015) Binary 2in1 vectors improve in planta (co)localization and dynamic protein interaction studies. *Plant Physiol* 168(3):776–787.
57. Spitzer M, Wildenhain J, Rappsilber J, Tyers M (2014) BoxPlotR: A web tool for generation of box plots. *Nat Methods* 11(2):121–122.
58. Grossmann G, et al. (2012) Time-lapse fluorescence imaging of Arabidopsis root growth with rapid manipulation of the root environment using the RootChip. *J Vis Exp* 65:pii:4290.
59. Schindelin J, et al. (2012) Fiji: An open-source platform for biological-image analysis. *Nat Methods* 9(7):676–682.
60. Jiang L, et al. (2005) VANGUARD1 encodes a pectin methylesterase that enhances pollen tube growth in the Arabidopsis style and transmitting tract. *Plant Cell* 17(2):584–596.
61. Boavida LC, McCormick S (2007) Temperature as a determinant factor for increased and reproducible in vitro pollen germination in Arabidopsis thaliana. *Plant J* 52(3):570–582.
62. Roppolo D, et al. (2011) A novel protein family mediates Casparian strip formation in the endodermis. *Nature* 473(7347):380–383.
63. Tokuyasu KT (1989) Use of poly(vinylpyrrolidone) and poly(vinyl alcohol) for cryoultramicrotomy. *Histochem J* 21(3):163–171.
64. Park M, Touihri S, Müller I, Mayer U, Jürgens G (2012) Sec1/Munc18 protein stabilizes fusion-competent syntaxin for membrane fusion in Arabidopsis cytokinesis. *Dev Cell* 22(5):989–1000.
65. Husbands AY, Benkovics AH, Nogueira FT, Lodha M, Timmermans MC (2015) The ASYMMETRIC LEAVES complex employs multiple modes of regulation to affect adaxial-abaxial patterning and leaf complexity. *Plant Cell* 27(12):3321–3335.
66. Loqué D, Lalonde S, Looger LL, von Wirén N, Frommer WB (2007) A cytosolic trans-activation domain essential for ammonium uptake. *Nature* 446(7132):195–198.
67. Rivera-Monroy J, et al. (2016) Mice lacking WRB reveal differential biogenesis requirements of tail-anchored proteins in vivo. *Sci Rep* 6:39464.
68. Aviram N, et al. (2016) The SND proteins constitute an alternative targeting route to the endoplasmic reticulum. *Nature* 540(7631):134–138.
69. Srivistava R, Zalisko BE, Keenan RJ, Howell SH (December 6, 2016) The GET system inserts the tail-anchored SYP72 protein into endoplasmic reticulum membranes. *Plant Physiol*, 10.1104/pp.16.00928.